Available online at www.sciencedirect.com

ScienceDirect

Procedia Manufacturing 34 (2019) 780–788

Procedia MANUFACTURING

www.elsevier.com/locate/procedia

47th SME North American Manufacturing Research Conference, Penn State Behrend Erie, Pennsylvania, 2019

Wear of structural oxide ceramics produced through additive manufacturing

Jessica Schiltz[a,*], Andrew Rosenberger[b], Todd Render[b], Bernice Aboud Gatrell[c], Haibo Qu[b], Colton Steiner[c], Paul McGinn[c], Steven Schmid[a,*]

[a]*Dept. of Aerospace & Mechanical Engineering, University of Notre Dame, Notre Dame, IN 46556, USA*
[b]*DePuy Synthes, Johnson & Johnson Co., Warsaw, IN, 46582, USA*
[c]*3D Printing COE, Johnson & Johnson Co., Warsaw, IN 46582, USA*
[d]*Dept. of Chemical & Biomolecular Engineering, University of Notre Dame, Notre Dame, IN 46556, USA*
*Corresponding author. Tel.: +1-574-631-1899 ; *E-mail address:* jschiltz@nd.edu

Abstract

Ceramics have exceptional tribological performance in high wear applications, but susceptibility to brittle fracture requires expensive post-processing, including hot isostatic pressing and polishing. Consequently, additive manufacturing (AM) represents a collection of potentially cost-saving approaches for ceramic production. AM technologies have been demonstrated for oxide ceramics, but the performance of self-mated AM materials remains unknown and underscores a critical knowledge gap. Alumina and zirconia pins produced with photo-polymerization, binder-jetting, or material-jetting were obtained. For each fabrication method, the average wear coefficient was determined using pin-on-disk testing. Conventionally pressed and sintered ceramics were applied as counterface surfaces and controls. The manufacturing approach did not demonstrate differences in wear coefficient for zirconia. However, photopolymerized alumina was shown to outperform material-matched binder-jetted and conventional pin-disk tribopairs. Starting surface roughness and bulk density were found to correlate volumetric wear. Characterization of the AM ceramics revealed that photo-polymerization and material-jetting were capable of dense and refined microstructures. Evaluations indicate that ceramics produced with photo-polymerization and certain powder-bed AM approaches meet and exceed conventional ceramics, supporting the expansion of AM ceramic applications.

Keywords: additive manufacturing; alumina, zirconia; tribology; photo-polymerization; wear coefficients; pin-on-disk

1. Introduction

For decades, technical ceramics have been the preferred substrate for bearings and wear applications. Ceramics are comprised of ionic bonds whose highly electronegative character confer the high strength, hardness, tolerance in elevated temperatures, and corrosion resistance that enhance wear performance [1]. But though ceramics demonstrate exceptional mechanical and tribological properties, ceramic parts are brittle and highly sensitive to defects. As a result, post-processing including final machining must be carefully controlled and the use of hot-isostatic pressing (HIP) is often employed to refine and homogenize the microstructure [2]. Consequently, these secondary operations are time and cost-intensive, and can account for well over 50% of the ceramic component cost [3]. The high costs associated with traditional ceramic fabrication, notably for part volumes associated with research or prototyping, has encouraged interest in identifying novel approaches capable of producing technical ceramics.

Nomenclature

ATZ	alumina toughened zirconia
AM	additive manufacturing
Al_2O_3	alumina
CP	Conventionally processed / commercial pure
TCP	tricalcium phosphate
PBF	powder bed fusion

2351-9789
10.1016/j.promfg.2019.06.206

DED	Directed energy deposition
R_a	average surface roughness
P_{poly}	photo-polymerization
Bjet	binder-jetting
Mjet	material-jetting
L	net load, N
V	volumetric wear, mm3
S	sliding distance, m
H	hardness, Vickers
Mc	million of cycles
ZrO_2	zirconia

1.1. Overview and advantages of AM

Historically, advancements in ceramic processing have been challenging. Conventional manufacturing, encompassing bulk-forming techniques, have limited production adaptations and poor design flexibility, which are further hindered by tooling costs and lead times. Alternatively, improved economics and process agility are touted for additive manufacturing (AM) in the production of one-off components and volumes suitable for investigative efforts. AM collectively describes software-driven fabrication methods that translate digital representations of three-dimensional parts into physical space through the layer-wise build-up of material, without the use of tooling [4]. Of the seven AM families, extrusion, photo-polymerization, material-jetting, and powder-bed approaches among others, have been described for ceramic production [5,6]. Commercial AM machines that offer qualified ceramic feedstocks primarily fall in the latter three categories (Table 1).

Table 1. Commercial monolithic AM ceramic solutions available to the U.S. market. *Note:** Xjet Al_2O_3 was announced in Nov. 2018.

Company	Machine	AM-approach	Qualified Material Offerings
Admatec BV Europe	Admaflex	P_{poly}	Al_2O_3, ZrO_2, SiO_2, ATZ, SiO_2-sand
Lithoz GmbH	CeraFab	P_{poly}	Al_2O_3, ZrO_2, Si_3N_4, SiO_2, TCP
3DCeram	Ceramaker	P_{poly}	Al_2O_3, ZrO_2, ATZ,
Xjet	Carmel	Mjet	ZrO_2, Al_2O_3*
Johnson Matthey	PixDro	Bjet	Al_2O_3
ExOne	M-flex, Innovent etc.	Bjet	$ZrSiO_4$, Al_2O_3, & SiO_2 foundry sands

Photo-polymerization (P_{poly}) utilizes powder suspensions, or slurries, containing light-sensitive monomers that are selectively cured with either a translating laser, also known as stereolithography, area light exposure, or digital mask projection. These material processes require careful optimization to ensure each viscous layer is completely polymerized. P_{poly} can achieve extremely fine resolution, but the thermodynamics of curing photosensitive monomers can result in geometric inaccuracies based on build directions [7,8]. This is often rectified with manual or automatic oversizing to account for shrinkage following firing and final-machining. Furthermore, complete burn-out of the chemical binder is distance-limited, places similar restrictions on wall thickness and part size as ceramic injection molding [9]. Material-jetting (Mjet) technologies rely on low viscosity feedstocks which is simultaneously cured either through thermal or lithography resulting in reduced cleaning time compared to photopolymerization, and higher resolution relative to extrusion AM. Nanoparticle jetting was developed as an Mjet subset, which incorporates nanoparticles into a liquid feedstock. This chemical carrier is pyrolyzed in a high temperature chamber to permit the bulk-sintering of particles and achieve complete densification. Use of nanoparticles confers superior mechanical properties by achieving refined sintered microstructures, but nano-sized powders can agglomerate and result in non-homogeneous compositions [10]. Powder bed fusion AM encompasses binder-jetting (Bjet) and laser-based sintering. Binder-jetting, is the selective application of an inorganic polymeric glue, while laser-sintering relies on a focused energy source to heat the particles to the melting point. For powder bed technologies the surrounding loose powder eliminates the need for support material. Cost-effective, and often more flexible in terms of fusion, powder-bed AM is considered to have higher scalability for larger production volumes. This technology also has fewer limitations on macro-sized features and larger wall thicknesses, since only minimal binder is applied to hold the part shape. However, surface finish and feature resolution remain challenges for powder bed processes given the physics associated with laser sintering and liquid droplets disrupting power layer [11–13]. A secondary concern with binder-jetting is the production high-density parts. In powder bed methods, particle size is limited to typically half of the layer-thickness, where the powder size distribution is governed by the ability of the roller or wipe mechanism to achieve a uniform layer [14].

1.2. Success with AM ceramic approaches

Today AM is a relatively ubiquitous process that has received considerable attention for metal and polymer consolidation but has not produced much success with technical ceramics. Industrial ceramics like, alumina (Al_2O_3) and zirconia (ZrO_2), present a persistent challenge for AM, as laser-based solid-state sintering struggles to produce fully-dense parts, in part due to ceramic-laser incompatibility, where the steep thermal gradients, and the materials' poor coefficient of thermal expansion leads to high residual stresses within the part [15]. Successful attempts at monolithic AM ceramics have utilized absorption additives and pre-heating techniques to mitigate crack formation, but have reported extremely poor surface finish due to uncontrolled melting [16–18]. As such, prevailing commercial solutions are inspired by traditional ceramic processing in the production of green body (Table 1). Consequently, these methods face similar challenges to conventional powder injection molding, wherein shrinkage and warpage are highly dependent on processing variables [19–21]. But despite the difficulties associated with the AM ceramic approaches, the reduction in the time and cost for functional prototyping and small lot production remain compelling reasons to advance AM ceramic developments.

1.3. Wear evaluations of AM materials

Confidence in structural AM materials has become contingent upon demonstrating that comparable properties are achieved relative to traditionally-manufactured parts. Today, density, hardness, and strength of AM ceramics evaluations are available, but few publications have investigated the wear of any AM materials at all. Furthermore, reports that include tribological testing have been focused on metals [22–24] or polymers [25,26] (Table 2). AM wear evaluations that reference ceramic-variants are limited to ceramic coatings [27,28] or bulk ceramic-additives in metal-matrix [29,30] or plastic [31] composites. The current landscape of AM tribology highlights the absence of monolithic ceramics, limited consideration of the AM parameters, large variation in experimental set-up, and the use of non-material matched surfaces as the counterface.

Table 2. Tribological evaluations of AM materials. Reported wear studies of various AM materials are primarily metals and polymers.

Ref.	AM Approach	AM Material	Counter-face	Load	Speed	Distance
[29]	PBF, DMLS™	Fe-Ni & TiC (block)	Steel (cylinder)	40 N	0.6 m/s	*n.r.*
[23]	PBF, SLS™	Fe-C (pin)	Steel (disk)	2/6 kg	0.58/4 m/s	*n.r.*
[30]	PBF, SLM™	Al (disk)	Steel (ball)	3N	560 rpm, 15 min	6 km
[24]	PBF, SLM™	Steel (ring)	Brass & Steel (ring)	3.3-10kN	10 rpm 30 min	21.7 m
[32]	PBF, EBM™	Ti (flat)	Ti (ball)	variable	100 µm/s, 30min	*n.r.*
[25]	Extrusion	ABS (pin)	Fe (flat)	35 N	8.4 m/s, 60min	*n.r.*
[26]	Extrusion	PLA (ring)	PLA (ring)	250/500 N	250/300 rpm, ~150sec	*n.r.*
[27]	DED, LENS™	Si-N coated Ti (flat)	Al_2O_3 (ball)	7 N	1200 mm/min	1 km
[28]	DED, LENS™	SiO_2 coated Ti (flat)	Steel & WC (ball)	10 N	1200 mm/min	1 km

Therefore, significant opportunities exist in the evaluation of AM monolithic ceramic-on-ceramic wear. Screening of self-mated AM ceramics is critical the expansion and development of novel wear- and fracture-resistant ceramics for various tribological applications. The present study investigates the wear behavior of Al_2O_3 and ZrO_2 fabricated with three AM approaches relative to non-HIPed pressed and sintered controls. Relevant properties to tribological performance are reported to provide context to the calculated wear coefficients.

2. Materials & Methodology

2.1. Wear test specimens

A comprehensive search of monolithic ceramic AM suppliers was performed. The study identified two P_{poly} vendors (Admatec Europe BV, The Netherlands & Lithoz GmbH, Austria), one Mjet vendor (Xjet, Israel), one Bjet vendor (Johnson Matthey, United Kingdom), and one conventional manufacturer (CoorsTek, Golden, Colorado). At the time of procurement both Al_2O_3 and ZrO_2 feedstocks were available by only the two P_{poly} vendors. Only one ceramic was purchased by the Bjet (Al_2O_3) and Mjet (ZrO_2) vendors. Spherically tipped Ø1/8" [3.18 mm] pins were procured from the P_{poly} and Mjet groups, and Ø3/8" [9.53 mm] pins were obtained from the Bjet vendor and the conventionally processed (CP) supplier (Fig 1). The larger diameter, in accordance to the ASTM recommendations, was initially requested from all vendors. However, both P_{poly} suppliers recommended a maximum wall thickness of 4-5 mm to achieve complete debinding and prevent sub-optimal material properties. Though the Mjet vendor could provide the larger diameter specimen, smaller diameter parts were used to provide statistical comparison (n=2). For all tests CP disks (Ø1-3/8" [34.9 mm]) were used as the wear flat. CP Al_2O_3 disks had R_a of 0.36 ± 0.11 µm and Hv9.8 of 15.3 ± 0.91 GPa, while CP ZrO_2 had an R_a of 0.19 ± 0.01 µm and Hv9.8 of 12.4 ± 0.06 GPa. Processing inputs, including starting size of the feedstock material, solids loading, and sintering time, are well recognized to affect resultant part microstructure and therefore were documented (Table 3).

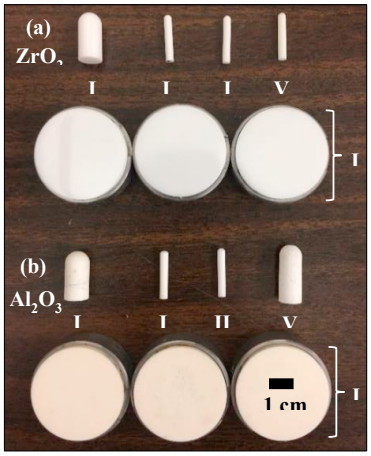

Fig. 1. (a) ZrO_2 & (b) Al_2O_3 parts from (i) CP (Coorstek), (ii) $P_{poly}1$ (Lithoz), (iii) $P_{poly}2$ (Admatec), (vi) Mjet (Xjet), and (v) Bjet (Johnson Matthey).

Table 3. AM vendor processing parameters. Particle size was notably smaller for P_{poly} vendors compared to Bjet, but solids loading was equivalent. n = 3 for all vendors except Mjet, n = 2. Specific binders could not be provided.

Vendor	Matl.	Particle Size	Sintering		Solids loading	Layer thickness
		µm	*(°C)*	*(hr)*	*%*	*µm*
$P_{poly}1$ (Lithoz)	Al_2O_3	0.05-1.0	1600	2	60	25
	ZrO_2	0.05-1.0	1450	2	40-45	
$P_{poly}2$ (Admatec)	Al_2O_3	~0.010	~1620	1	40-50	30
	ZrO_2	0.090	~1525	1	40-50	
Bjet (J. Matthey)	Al_2O_3	40.0	1400	*n.r.*	50	100
Mjet (Xjet)	ZrO_2	0.030 - 0.090	*n.r.*	12, one-step	60	10

The two P_{poly} groups fabricated specimens with the spherical tip vertically in the +z-direction, such that the laminar architecture ran perpendicular to compressive load. The Bjet and Mjet vendors oriented the specimens horizontally in the bed, to conserve build material, where the long-axis of the pin was perpendicular to the build- or +z-direction (Fig. 2). Wear specimens were tested as-received to evaluate all ceramics in a non-polished state, simulating an aggressive wear scenario and ensure measurable changes would be observed.

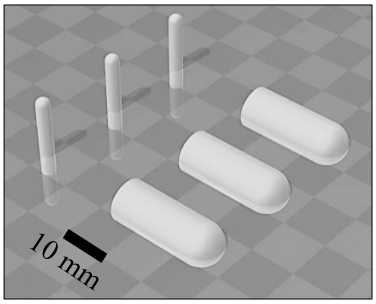

Fig. 2. Specimen build orientation was vendor-specific due to cost constraints. The two P_{poly} wear pins were oriented vertically (a), while the Bjet and Mjet pins were oriented horizontally (b), perpendicular to the build direction.

2.2. Specimen & material characterization

The as-received printed surface finish can highly influence the wear response [33,34]. The initial arithmetic roughness (R_a) of each material was assessed using a stylus profilometer (DektakXT Bruker, Tucson, AZ). A 2 µm diamond tip was used to map a 50 µm x 50 µm area on three locations of a single sample for three independent samples, to obtain R_a. All measurements were taken in the plane of wear regardless of build orientation. The volumetric porosity and bulk density of all Al_2O_3 and ZrO_2 coupons (n=5) were assessed using the standard Archimedes approach [35]. Samples were then ground with successive grits (400, 600, 800, 1200) then polished with 1µm diamond paste, 0.05µm and 0.02µm colloidal silica. Hardness of ZrO_2 and Al_2O_3 was evaluated from the average of ten indents on three independent P_{poly} and CP specimens at 1kgf (9.8 N) for 15 sec on a micro-indentation hardness tester (Leco M-400, St. Joseph, Michigan) [36]. Polished P_{poly}, CP, and Mjet samples were thermally etched in a furnace for 1400°C for 20-30 minutes to reveal grain boundaries, visualized with scanning electron microscopy (SEM). Grain size analysis was performed with the circular-intersection method [37].

2.3. Tribological testing

Pins from the five manufacturing groups were worn against material-matched CP disks on a six-station pin-on-disk tribometer (AMTI, Watertown, NJ). The spherical tip of each pin was fixtured such a dynamic load (21N, average) was applied orthogonal to the counterface surface as the pin travelled along 10 mm square track (Fig. 3). The loads were load was scaled such that all materials, regardless of geometries, experience contact pressures/stresses in the same order of magnitude. The resultant Hertzian contact was resolved to be 2.7 GPa for the Ø1/8" [3.18 mm] pin and 1.3 GPa for the Ø3/8" [9.53 mm] pin. These contact stresses make the wear tests relevant for bearings, gears and other machinery elements, as well as dental applications and other machine elements, given that the stresses are higher than typically encountered in machinery applications [38]. Ceramics exhibit wear at much lower volumes compared to metals and polymers, and thus the high contact pressures created a wear scenario that ensured that debris loss comparisons would be made. The pin movement was lubricated with deionized water (dIH_2O) held at 37°C±2°C. Six longitudinal timepoints of 0.33 million cycles (Mc) were evaluated, for a total of 1.98 Mc at 1.6 Hz, equating to ~80 km. At each time interval, pin-disk pairings were ultrasonically cleaned and the resultant wear scar on each pin was examined under optical microscopy [39]. Images were taken at 50-100X magnification and measured with NIH Image J software.

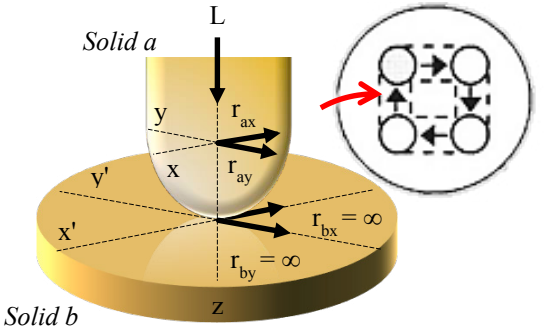

Fig. 3. Pin-on-disk schematic. A dynamic load, L, is applied as the pin travels a 10mm path. Contact mechanics calculated pressures within the same order of magnitude for the different sized pins [5].

Volumetric wear can be related to test inputs via the Archard Wear law,

$$V = k \frac{L S}{3 H} \quad (1)$$

where k, is the dimensionless wear factor, H, is Brinell macro-hardness, V, is the volumetric wear, L, is the net force applied, and S, is the total sliding distance [40]. Accurate Brinell hardness values are difficult to obtain for ceramics, so Eq. (1) can be rearranged, such that the wear coefficient, κ, incorporates, H, hardness,

$$\kappa = \frac{k}{H} = \frac{3 V}{L S} \quad (2)$$

permitting a general assessment of the wear response.

2.4. Statistical Analysis

A single factor Analysis of Variance (ANOVA) or the appropriate equivalent non-parametric test was used to assess statistical significance for the evaluated material properties (α<0.05). Multiple comparison tests, such as a Tukey post-test was applied as necessary to identify differences between the

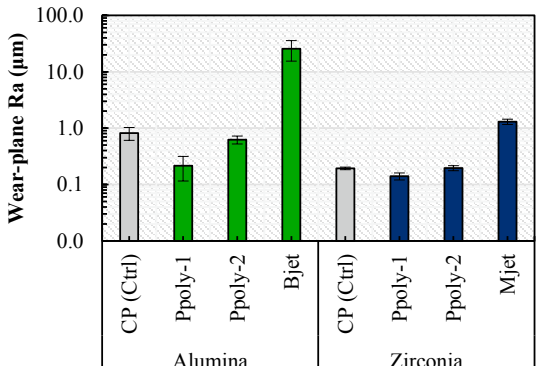

Fig. 4. Average roughness (Ra) of the wear plane of AM pins. Bjet R_a was more than an order of magnitude greater than all other processes.

five manufacturing approaches. A Pearson's correlation test was performed to establish relationships between the measured AM material properties and wear performance.

3. Results

3.1. AM ceramic specimen characterization

As-received surface finish is important to compare because roughness of as-built AM parts is typically higher than that used in machinery elements. Bjet, as a powder-bed technology, had a visibly rougher starting surface compared P_{poly} and Mjet technologies (Fig. 4). This is attributed to a much larger particle size of the ceramic feedstock (Table 3). When compared to the CP controls, a significant difference in porosity was identified across manufacturing approach for Al_2O_3, but not ZrO_2 ($p=0.78$) (Fig. 5). A subsequent Tukey test ($\omega_{min} = 0.08$) of the four Al_2O_3 groups revealed that only $P_{poly}1$ Al_2O_3 was comparable to the CP Al_2O_3 control, as $P_{poly}2$ and Bjet Al_2O_3 had significantly lower densities. This was expected for the Bjet group which was found to have a volumetric porosity averaging higher than 40% (Fig. 5) However, though $P_{poly}2$ was observed to have a significantly lower density, a trend towards non-significance could be argued ($\omega_{min} = 0.13$). However, given that the statistical power for both Al_2O_3 and ZrO_2 tests was low ($1-\beta<0.15$), additional samples are be necessary to conclude that meaningful differences exist.

Grain size analysis is often important for wear related metrics. Grain measurements revealed that the average grain size was between 2–5 µm for Al_2O_3, and between 0.3–0.6 µm for ZrO_2 (Table 4). SEM images of thermally-etched surfaces reveal that Al_2O_3 grains are darker in color, are angular in shape, and have triangular porosity (Fig. 6). Quantitative counts were not reported for Bjet samples, since the high levels of porosity of each pin prevented a suitably large surface area for etching and analysis. However, SEM micrographs of the Bjet wear surface depict faint outlines of much larger (~15 µm) irregular grains, which contain porosity within and along grain boundaries (Fig. 6d). Though porosity is similarly located for

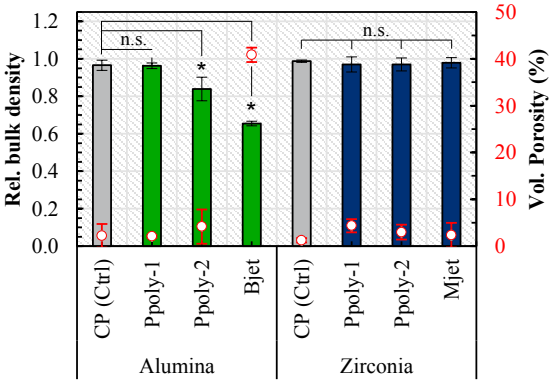

Fig. 5. Relative bulk density for AM specimens. All ZrO_2 specimens were comparable to the CP controls, while Bjet Al_2O_3 had the lowest density compared to the CP and P_{poly} pins. (n.s., not significant and * = $p<0.05$).

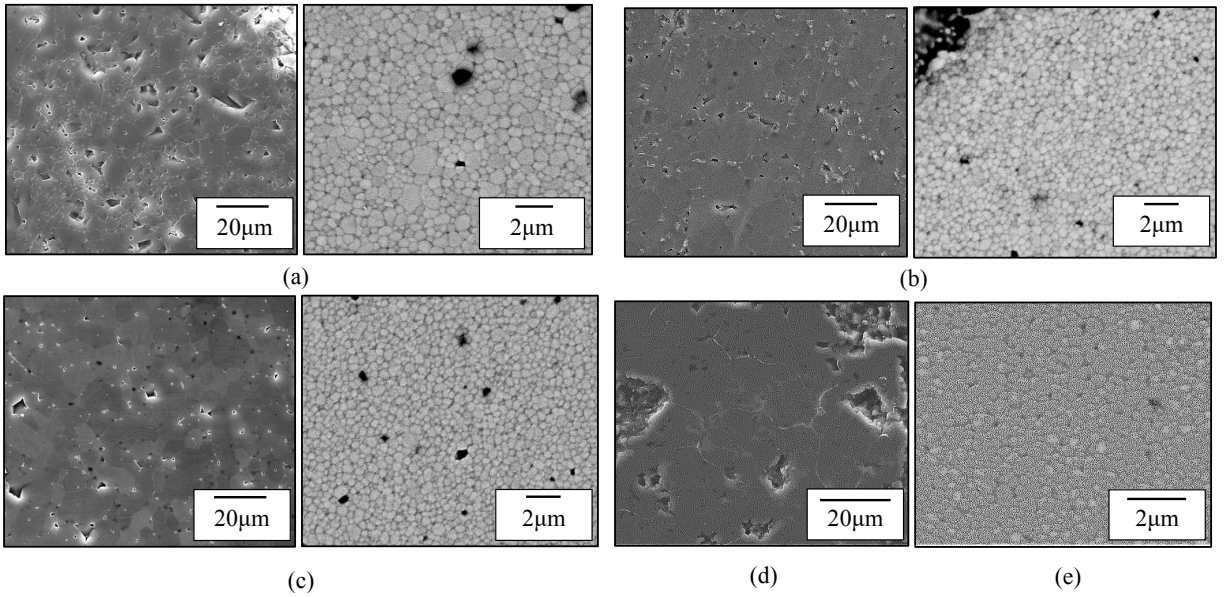

Fig. 6. Qualitative SEM images of Al_2O_3 (left) and ZrO_2 grains (right) for (a) CP controls, (b) Ppoly-1, (c) Ppoly-2, (d) Bjet Al_2O_3, and (e) Mjet ZrO_2.

CP and Ppoly$_2$ Al_2O_3, $P_{poly}1$ Al_2O_3 porosity occurs primarily along grain boundaries and appears was lower in magnitude, supporting the Archimedes measurements (Fig. 6b & Fig. 5). However, the grain size of the $P_{poly}1$ Al_2O_3 are larger compared to CP and $P_{poly}2$. ZrO_2 grains are lighter in color, circular and smaller in size compared to Al_2O_3. Porosity appears to be similar in size to the grain diameters.

Table 4. Quantitative grain size measurements. Grains for Al_2O_3 ranged between 1.5 and 3.0μm, while submicron grains were preserved for ZrO_2. Averages were taken from atleast three images, from two independent specimens.

Average grain diameter, *d* (μm)							
Al_2O_3				ZrO_2			
CP	1.70	±	0.28	CP	0.57	±	0.01
$P_{poly}1$	4.93	±	0.61	$P_{poly}1$	0.37	±	0.02
$P_{poly}2$	2.07	±	0.18	$P_{poly}2$	0.39	±	0.03
Bjet	*n.r.*	±	*n.r.*	Mjet	0.32	±	0.10

3.2. AM ceramic wear comparisons

For hard-on-hard bearings, the mass of wear debris can be smaller than the error associated with gravimetric equipment [41]. As such, the wear scar was measured using NIH Image J Software from optical micrographs of each hemispherical tipped pin to reduce measurement uncertainty (Fig. 7) [39]. Prior to testing, the laminar architecture of the P_{poly} ceramic pins can be observed (Fig 7-II & -III). Approximately 80km (1.98 million cycles) were carried out. Wear loss is visualized as the gradual widening of a circular scar on the top of each pin throughout the six timepoints. Ceramic on ceramic articulation under loading resulted in the self-polishing of the scar to a mirror-like finish. When volumetric wear was used to calculate the wear coefficient, Bjet Al_2O_3 had the lowest wear resistance followed by CP Al_2O_3 and then $P_{poly}2$ Al_2O_3 (Table 5). However, due to high standard deviation, no significant difference measured across the four Al_2O_3 groups (*p=0.11*). The four ZrO_2 groups demonstrated higher wear resistance compared to Al_2O_3, but similarly exhibited no difference in wear response across the four manufacturing methods (*p=0.77*)

Table 5. Wear coefficient comparisons of various AM oxide ceramics.

Average wear coefficient, κ (mm^3/Nm)							
Al_2O_3				ZrO_2			
CP	2.3×10^{-7}	±	1.1×10^{-7}	CP	3.9×10^{-8}	±	3.2×10^{-8}
$P_{poly}1$	1.6×10^{-8}	±	1.5×10^{-8}	$P_{poly}1$	2.2×10^{-8}	±	2.7×10^{-8}
$P_{poly}2$	7.5×10^{-8}	±	3.6×10^{-8}	$P_{poly}2$	2.4×10^{-8}	±	2.6×10^{-8}
Bjet	6.5×10^{-7}	±	5.8×10^{-7}	Mjet	2.7×10^{-8}	±	2.4×10^{-8}
p-value	0.11			*p-value*	0.77		

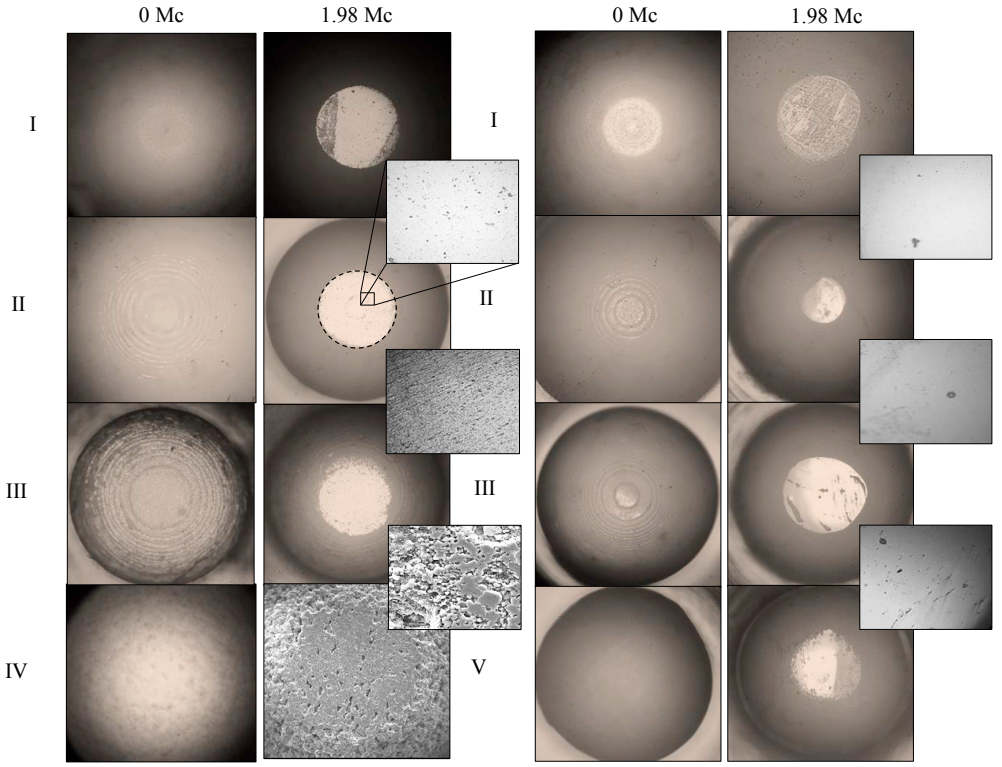

Fig. 7. Representative micrographs of (a) Al_2O_3 and (b) ZrO_2 wear-scar progression, at 50X magnification, for (i) CP, (ii) $P_{poly}1$, (iii) $P_{poly}2$, (iv) Bjet, and (v) Mjet technologies. As the hemispherical pin articulated against the wear flat, a self-polished circle gradually formed. Inset images of AM pins are at 100x mag. Note: (a-IV, Bjet) image and inset at 1.98 Mc are SEM images, for higher depth resolution, 50x and 1500x, respectively.

4. Discussion

4.1. Wear analysis

The wear coefficient normalizes wear tests, permitting general screening for wear resistance. However, caution must be used when comparing wear factors to those determined outside the present study, as experimental outcomes are highly dependent on test configuration and selected parameters. However, the wear coefficient has long been established as a robust metric for comparing long-term behavior of different material pairings within and across studies [42]. The wear results suggest that P_{poly} and Mjet technologies produced dense ceramics that have functional wear performance comparable to CP controls. Of the two ceramics, ZrO_2 demonstrated improved wear behavior compared to Al_2O_3, despite having lower hardness (Fig. 8). When comparing with respect to manufacturing method, the both $P_{poly}1$ ceramics had a higher average hardness and lower initial R_a values, could explain the improved wear resistance over the CP controls.

Under aqueous-lubricated conditions, all reported coefficients were within a magnitude of 10^{-8}–10^{-7}, which is lower than the accepted indicator of a wear-resistant material (10^{-6} mm^3/Nm). Al_2O_3 and ZrO_2 CP pins reported a wear coefficient of 2.3×10^{-7} and 3.9×10^{-8} mm^3/Nm, respectively. This agrees with previous values reported for self-mated ceramic-on-ceramic wear applied ranging between 1-3 GPa [43]. The CP ceramic wear results therefore suggest the experimental set-up was reasonable and produced wear conditions that would permit comparisons.

The AM ZrO_2 groups were shown to wear comparably to the material-matched controls. Magnified surfaces of AM ZrO_2 wear-scars, etched under thermal conditions, support the wear results, as all surfaces were visually similar (Fig.7b). Though, Mjet ZrO_2 did exhibit greater porosity and surface features compared to the other two AM groups, bulk density and grain size were found to be equivalent.

For the Al_2O_3 groups, $P_{poly}1$ exhibited the highest wear resistance, while the wear coefficient for Bjet Al_2O_3 was calculated higher than CP Al_2O_3. This was expected as, strength-related properties, including wear, are known to be influenced by material density and surface quality. From the micrographs of AM Al_2O_3 wear-scars provide a potential explanation why $P_{poly}2$ Al_2O_3 demonstrate higher wear compared to the other P_{poly} process, as the polished surface of the $P_{poly}2$ Al_2O_3 retained a striated texture (Fig. 7a-II). Surface features such as pores and texture can be critical to tribological evaluation as the pins interact with the counterface. High pressure as the two surface articulate can result in heighted stress concentrations or increased asperity contact, which can subsequently lead to increased damage and cracking [44]. The test results suggest that initial wear-plane R_a values were strongly correlated to wear response ($r = 0.95$). This correlation was stronger than relative density, and by extension the volumetric porosity ($r = -0.88$), however the measured inverse correlation is still considered a strong predictor of tribological performance. In other words, AM wear behaviour adheres to the current canon that holds that lower initial surface roughness and higher relative density results in improved wear-resistance. Of note, Bjet had the largest surface roughness, which is an accepted trade-off for powder-bed fusion approaches. Extreme roughness (25μm+) seen for Bjet coupons is understood to increase wear given the larger volume of asperities that interact with the counter-body which produces a sharper wear transition as a result of third-body polishing. Though previous work have shown that cavities and porosity improve lubricated wear conditions by serving as reservoirs for collected debris, the uneven edges and larger grains would generate stress concentrations that lead to crack development and production of fatigue spall, exacerbating third-body wear (Fig. 6d) [45]. However, though Bjet parts would require development to utilize a wear-resistant ceramic, the technology is not without use. For example, powder-bed printing of investment casts or ceramic filters for catalysis devices benefit from high volumetric porosity for infiltration and increased surface area.

Refined grain size is has also been correlated with improved wear response [46]. However, a significant negative correlation was observed between wear and grain size of Al_2O_3 ($r = -0.78$), suggesting that smaller grain sizes produced higher wear. This is contrary to general wear behavior which usually improves with smaller grain sizes, exemplified by the slight positive correlation depicted by the ZrO_2 groups ($r = 0.32$).

The objective of this work is to screen the wear behavior of ceramics fabricated with five different AM technologies. As such, only three specimens were tested for the two ceramic oxides. Therefore, standard deviations greater or equal to half the average were observed for nearly all material groups apart from CP and $P_{poly}2$ Al_2O_3 (Table 5). Significant scatter is common in wear testing, and one in five ceramic wear systems report samples with outliers which deviate drastically from the mean [47]. However, having identified P_{poly} and Mjet as strong candidates in the production of wear-resistant ceramics additional wear studies will require increase sample size.

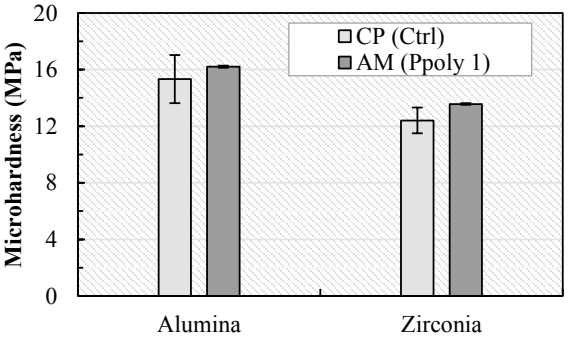

Fig. 8. Vicker's microhardness test results for CP and $P_{poly}1$ pins. ZrO_2 was ~2-4 GPa softer than Al_2O_3, but still produced very low wear.

4.2. AM processing variation and wear behavior considerations

Wear is a complicated phenomenon, where a variety of mechanisms and factors such as material properties and test conditions contribute to the measurement. For instance, though all pins were originally requested with dimensions that adhered to standards and were compatible with tribometer fixtures, P_{poly}

ceramic suppliers recommended scaling down the part diameter to prevent confounding results from sub-optimal materials. P_{poly} approaches follow traditional debinding profiles and thus incomplete removal of the resin or binders can induce cracking and warpage when the furnace ramps to the extreme temperatures required to sintered ceramics [48]. To account for the smaller pins, the load was scaled such that the Hertzian contact stress experienced by all pins was the same order of magnitude (1.3-2.7 GPa). This was determined to be acceptable for preliminary wear benchmarking of AM ceramics. Although the smaller pins would be anticipated to produce higher wear due to nominally higher stresses, $P_{poly}2$ Al_2O_3, Ø1/8" had reasonably equivalent porosity and R_a (4.17% and 0.62 µm), to Ø3/8" CP Al_2O_3 (2.12% and 0.82 µm). Subsequently, both geometries produced similar wear coefficients (0.8×10^{-7} and 2.0×10^{-7} mm^3/Nm, respectively). Additionally, since all AM pins were tested in the as-received condition, in water-lubricated conditions, improved wear would be expected with controlled surface-finish and different lubricants. Non-aqueous lubricants are often paired with oxide ceramics, since earlier studies have reported a ten-fold increase in wear from hydro-initiated surface plasticity (the Rebinder effect) [49].

Another important consideration for AM parts is build orientation, which has been reported to affect strength-related properties since strength between lamination is assumed lower than the strength within a layer [50]. Vertical prints, though ideal for evaluation of properties within a material layer, were not feasible for all vendors at the low volumes of samples procured. However though, part orientation was not conserved for this study, the effect was expected to be mitigated by the extended duration of the wear test. An earlier investigation of P_{poly} ZrO_2 concluded that the anisotropic surface character was eliminated through polishing [51]. Removal of the as-built surface was observed after the very first time point, suggesting that a large percentage of the wear test occurred where the ceramic surfaces were highly polished (Fig 9). Additionally, though Mjet pins were printed horizontally, the similar density, grain size, and starting roughness to the vertically-printed P_{poly} and CP ZrO_2 specimens resulted in no significant effect on wear response. This agrees a wear study of laser-sintered Ti64 which reported no anisotropy with respect to wear response [32]. Thus, though additional testing with higher statistical sampling would be required to make clearer conclusions about print directionality on AM ceramic tribology, at present there appears to be no strong dependence on ceramic wear. Future studies will also need to focus on characterizing and resolving more timepoints associated with the initial wear stages to fully characterize AM ceramic tribology.

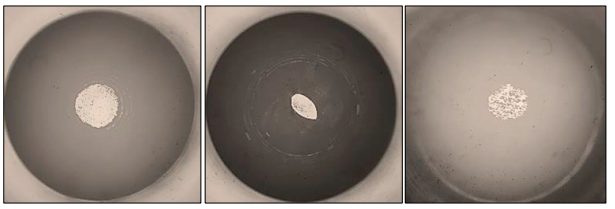

(a) (b) (c)

Fig. 9. Wear scars following the first timepoint, 0.33 Mc, for (a) $P_{poly}1$ Al_2O_3, (b) $P_{poly}2$ ZrO_2, and Mjet ZrO_2.

5. Conclusions

Water-lubricated wear of oxide ceramics pins fabricated with AM approaches were shown to have comparable wear to conventionally processed material-matched controls. Additive approaches are emerging as popular manufacturing alternatives in part to the flexibility in design and part production. Given that ceramics are employed in applications where longevity is desired, if AM ceramics demonstrate comparable wear rates to traditional methodologies, significant material and processing development opportunities arise. In this study, no advantage was shown in the use Bjet ceramics for high-wear applications without further process advancement and experimentation. On the other hand, photo-polymerization and material-jetting strategies are currently able to achieve parts with material properties of existing ceramic materials through high solids loading, refined powder size, and optimized sintering profiles. Thus, these AM strategies have strong indication that material development can be leveraged for further wear evaluations.

Acknowledgements

The authors would like to extend thanks to the ND Energy Materials Characterization Facility (MCF) for the use of the stylus profilometry unit and the DePuy Synthes Metallurgy Laboratory (Warsaw, IN) for facility use and staff training and technical support. The MCF is funded by the Sustainable Energy Initiative (SEI), which is part of the Center for Sustainable Energy at Notre Dame (ND Energy).

References

[1] P. Greil, Advanced Engineering Materials 4 (2002) 247–254.
[2] M.H. Bocanegra-Bernal, C. Domínguez-Rios, A. Garcia-Reyes, A. Aguilar-Elguezabal, J. Echeberria, A. Nevarez-Rascon, International Journal of Refractory Metals and Hard Materials 27 (2009) 900–906.
[3] F. Klocke, Journal of the European Ceramic Society 17 (1997) 457–465.
[4] A. Zocca, P. Colombo, C.M. Gomes, J. Günster, Journal of the American Ceramic Society 98 (2015) 1983–2001.
[5] Serope Kalpakjian, Steven Schmid, Manufacturing Processes for Engineering Materials, 6th ed., Pearsons Prentice Hall, 2016.
[6] ASTM F2792-12a, (2019) 3.
[7] S.P. Gentry, J.W. Halloran, Journal of the European Ceramic Society 33 (2013) 1981–1988.
[8] M.N. Islam, H. Gomer, S. Sacks, The International Journal of Advanced Manufacturing Technology 88 (2017) 3077–3087.
[9] B.H. Rosof, JOM 41 (1989) 13–16.
[10] D. Gu, H. Wang, G. Zhang, Metallurgical and Materials Transactions: Physical Metallurgy and Materials Science, A; New York 45 (2014) 464–476.
[11] A. Butscher, M. Bohner, N. Doebelin, L. Galea, O. Loeffel, R. Müller, Acta Biomaterialia 9 (2013) 5369–5378.
[12] M.J. Matthews, G. Guss, S.A. Khairallah, A.M. Rubenchik, P.J. Depond, W.E. King, Acta Materialia 114 (2016) 33–42.
[13] P. Bidare, I. Bitharas, R.M. Ward, M.M. Attallah, A.J. Moore, Acta Materialia 142 (2018) 107–120.
[14] A. Butscher, M. Bohner, C. Roth, A. Ernstberger, R. Heuberger, N. Doebelin, P. Rudolf von Rohr, R. Müller, Acta Biomaterialia 8 (2012) 373–385.
[15] J. Deckers, S. Meyers, J.P. Kruth, J. Vleugels, Physics Procedia 56 (2014) 117–124.
[16] J. Wilkes, Y.-C. Hagedorn, W. Meiners, K. Wissenbach, Rapid Prototyping Journal; Bradford 19 (2013) 51–57.
[17] E. Juste, F. Petit, V. Lardot, F. Cambier, Journal of Materials Research 29 (2014) 2086–2094.
[18] Q. Liu, Y. Danlos, B. Song, B. Zhang, S. Yin, H. Liao, Journal of Materials Processing Technology 222 (2015) 61–74.

[19] I. Shishkovsky, I. Yadroitsev, P. Bertrand, I. Smurov, Applied Surface Science 254 (2007) 966–970.
[20] M.C. Leu, S. Pattnaik, G.E. Hilmas, Intl SFF Symposium Proceedings (2010) 11.
[21] G. Mitteramskogler, R. Gmeiner, R. Felzmann, S. Gruber, C. Hofstetter, J. Stampfl, J. Ebert, W. Wachter, J. Laubersheimer, Additive Manufacturing 1–4 (2014) 110–118.
[22] S. Kumar, J.-P. Kruth, Advanced Engineering Materials 10 (2008) 750–753.
[23] K. Murali, A.N. Chatterjee, P. Saha, R. Palai, S. Kumar, S.K. Roy, P.K. Mishra, A.R. Choudhury, Journal of Materials Processing Technology 136 (2003) 179–185.
[24] Y. Zhu, J. Zou, X. Chen, H. Yang, Wear 350–351 (2016) 46–55.
[25] M. Dawoud, I. Taha, S.J. Ebeid, Materialwissenschaft Und Werkstofftechnik 46 (2015) 1185–1195.
[26] S. Perepelkina, P. Kovalenko, R. Pechenko, K. Makhmudova, Tribology in Industry 39 (2017) 519–526.
[27] Y. Zhang, H. Sahasrabudhe, A. Bandyopadhyay, Applied Surface Science 346 (2015) 428–437.
[28] B. Heer, A. Bandyopadhyay, Additive Manufacturing 23 (2018) 303–311.
[29] A. Gåård, P. Krakhmalev, J. Bergström, Journal of Alloys and Compounds 421 (2006) 166–171.
[30] D. Gu, H. Wang, D. Dai, F. Chang, W. Meiners, Y.-C. Hagedorn, K. Wissenbach, I. Kelbassa, R. Poprawe, Journal of Laser Applications 27 (2014) S17003.
[31] K. Boparai, R. Singh, H. Singh, Virtual and Physical Prototyping 10 (2015) 59–66.
[32] J.J. Ryu, S. Shrestha, G. Manogharan, J.K. Jung, Metals; Basel 8 (2018) 131.
[33] Y. Wang, S.M. Hsu, Wear 195 (1996) 90–99.
[34] Z. Maros, C. Felhő, Z. Vass, M.B. Maros, Materials Science Forum 812 (2015) 435–440.
[35] ASTM C373-17, ASTM International (2017) 6.
[36] ASTM C1327-15, ASTM International (2015) 10.
[37] ASTM E112-13, ASTM International (2013) 28.
[38] S. Schmid, B. Hamrock, B. Jacobson, Fundamentals of Machine Elements, 3rd ed., CRC Press Taylor & Francis Group, New York, 2014.
[39] ASTM G99-17, ASTM International (2017) 6.
[40] J.F. Archard, W. Hirst, Proc. R. Soc. Lond. A 236 (1956) 397–410.
[41] E. Serra, A. Tucci, L. Esposito, C. Piconi, Biomaterials 23 (2002) 1131–1137.
[42] E. Rabinowicz, Journal of Lubrication Technology 103 (1981) 188–196.
[43] S.M. Hsu, M.C. Shen, Wear 200 (1996) 154–175.
[44] O. O. Ajayi, K. C. Ludema, Wear 124 (1988) 237–257.
[45] M. Kalin, S. Jahanmir, Wear 255 (2003) 669–676.
[46] C.C. Wu, R.W. Rice, D. Johnson, B.A. Platt, in: W. Smothers (Ed.), Ceramic Engineering and Science Proceedings, John Wiley & Sons, Inc., Hoboken, NJ, USA, 1985, pp. 995–1011.
[47] S. Guicciardi, C. Melandri, F. Lucchini, G. de Portu, Wear 252 (2002) 1001–1006.
[48] C.-J. Bae, J.W. Halloran, International Journal of Applied Ceramic Technology 8 (2011) 1289–1295.
[49] I. Hutchings, Tribology: Friction and Wear of Engineering Materials, Edward Arnold, London, 1992.
[50] W. Harrer, M. Schwentenwein, T. Lube, R. Danzer, Journal of the European Ceramic Society 37 (2017) 4331–4338.
[51] H. Xing, B. Zou, S. Li, X. Fu, Ceramics International 43 (2017) 16340–16347.

.